BULLETIN OF THE POLISH ACADEMY OF SCIENCES
TECHNICAL SCIENCES, Vol. 69(5), 2021, Article number: e138817
DOI: 10.24425/bpasts.2021.138817

Charge dynamics of partial discharges explored applying a chopped sequence

Marek FLORKOWSKI*

AGH University of Science and Technology, Department of Electrical and Power Engineering, al. Mickiewicza 30, 30-059 Kraków, Poland

Abstract. Diagnostic methodologies are of fundamental importance for operational strategies of electrical devices, both in the power grid and in industrial applications. This paper reports about a novel approach based on partial discharge analysis applied to high voltage electrical insulation. Especially dynamics of charges deposited by partial discharges is explored applying a chopped sequence. The applications refer to microvoids occurring inside solid insulating systems or at the interfaces, such as delaminations at the electrodes. The experiments were carried out on embedded voids having distinctive wall dielectric materials. The underlying physical phenomena of post discharge charge transport are analyzed. The assessment is performed using phase-resolved partial discharge patterns acquired applying a chopped sequence. The chopped partial discharge (CPD) method provides quantitative insight into post discharge charge decay processes due to deposited and accumulated charges fluctuations. The assessment indicator is based on comparing partial discharge inception angle between chopped sequence and continuous run. The experiments have shown that materials with distinctive surface conductivity revealed adequately different charge decay time dynamics. The detailed analysis yields time constant of walls charge decay for insulating paper equal to 12 ms and cross-linked polyethylene 407 ms. The CPD method may be further used to investigate streamer physics inside bounded cavities in the form of voids. The presented method provides a quantitative approach for charge non-invasive decay assessment and offers high potential in future diagnostics applications.

Key words: partial discharges; chopped sequence; high voltage insulation; non-invasive diagnostics.

1. INTRODUCTION

The condition of high voltage (HV) insulation plays a crucial role in the reliable and resilient electrical power system. It refers to many grid components such as generators, transformers, power cables, insulators, substations apparatus, including gas insulated substations, insulators, and more power electronics-based equipment. This problem is also valid in industrial environments, e.g. motors and in emerging areas such as e-mobility, where the electrical insulation level has an increasing trend. High voltage insulation integrity is assessed using various complementary techniques, among which diagnostics based on partial discharges (PD) is essential. The physical mechanism of partial discharges, investigated over the last century, is an extremely complex and multidisciplinary topic. The imperfections inside HV insulating materials and their effects in high electric fields lead to insulation deterioration. The defects can assume a form of electric treeing in solid dielectric materials, microvoids or delaminations, and protrusions, microblades or floating particles in gaseous insulating systems. All cases mentioned above are revealed by the presence of partial discharges, which exhibit statistical character as a result of the interplay of several factors such as inception/extinction voltage, time lag, dielectric surface type influencing the decay of the deposited charges, and variations in discharge area in the void [1–6]. Surface charge dynamics has been studied extensively by many researchers, e.g. [7–27].

Significant research has been carried out on the decay processes [8–10, 14, 16, 24, 27] and associated material properties [11, 12, 20, 21]. Especially influence of surface conductivity on charge build-up was investigated [13, 22, 25]. There has been much research with respect to surface charge measurement, e.g. [17, 18, 23] and modeling, e.g. [7, 8, 15, 19, 20] – especially in the last few decades. The discharge transitions occurring in a void are often attributed to the memory effects that are associated with residual accumulated charges [13, 21, 23, 26]. In that context, insight into the microstructure of electrical insulation systems and an understanding of the associated underlying physical phenomena is a relevant research topic. An interesting observation based on the Pockels effect of surface charge decay in a void with a polyethylene film wall was described in [27]. The evaluated in the paper decay was in a range between 30 ms and 150 ms, depending on the polarity. The optical methods are very well suited for laboratory experiments; however, the transparent requirements for tested objected are limited in practical implementations.

This paper presents an application of novel methodology based on investigations of post-discharge charge decay in a dielectric void subjected to chopped partial discharge sequence [18, 28]. Unlike conventional methods used in high voltage diagnostics, which are based on continuous voltage application, the chopped sequence is aimed to reveal elements of PD dynamics and contribute to the explanation of the internal mechanisms. This new methodology is based on the application of

*e-mail: marek.florkowski@agh.edu.pl

Manuscript submitted 2021-06-17, revised 2021-07-22, initially accepted for publication 2021-08-08, published in October 2021

a repeating series of packets to a dielectric insulation system. Each packet is composed of a number of base waveforms followed by the delay time between subsequent packets. Then, the whole structure called epoch is repeated sequentially. The exemplary results in two kinds of voids embedded in the insulating materials are compared. The methodology is based on the phase-resolved PD patterns and provides a quantitative approach for charge non-invasive decay assessment.

2. PARTIAL DISCHARGE CHARGE DYNAMICS IN VOID

Gaseous microvoid represents one of the most typical defects occurring in a structure of high voltage insulation. Partial discharges are occurring in such inclusion, as illustrated in Fig. 1. Such defects can be localized in the different places of the HV insulation system, i.e. can be placed in bulk dielectric, on the interfaces or may form delaminations along the electrodes.

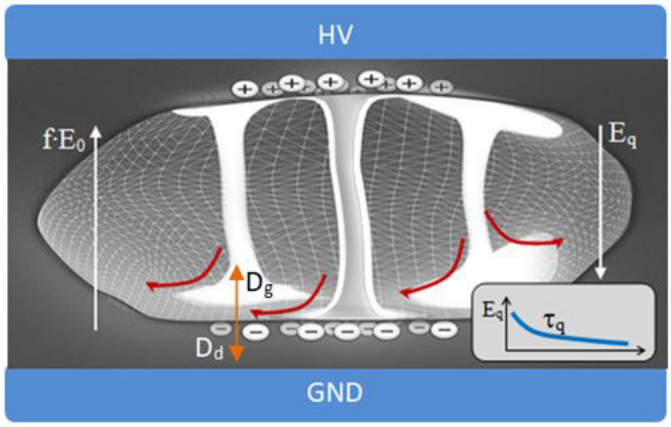

Fig. 1. Representation of void and decay time τ_q of field E_q due to different origins: fE_0 – background electric field in the void; D_g, D_d – displacement fields in gas and dielectric

Every PD event is associated with a charge transport and deposition on the void's walls. In that context, insight into the microstructure of a HV insulation material and the understanding of underlying physical phenomenon and processes is a relevant and actual research topic. It is known that partial discharges reveal the statistical character in a void due to an influence of several factors such as variation of inception voltage, time lag, fluctuation of the discharge area and surface/bulk phenomena such as charge transport [1, 2, 8, 28]. The latter one influences the decay process of deposited surface charges. Charge dynamics and associated memory effects have been studied extensively, e.g. [2, 8–12, 26, 29, 30]. The electric field E in the void is governed by Poisson equation:

$$\varepsilon_0 \nabla \cdot \varepsilon_r E = \rho_s + \rho_a \,, \tag{1}$$

where ε_0 is a vacuum dielectric permittivity, ε_r relative permittivity of the medium/material, ρ_s is a PD related space charge density and ρ_a a surface accumulated charge density. The space charge density ρ_s results from the net sum contribution of electrons n_e and both positive n_p and negative ions n_n present in the discharge, taking into account their polarity:

$$\rho_s = e\,(n_p - n_n - n_e)\,, \tag{2}$$

where e is an elementary charge.

The difference in the normal component (**n**) of dielectric displacement between the dielectric D_d and gaseous side D_g results in a surface charge density ρ_d:

$$\rho_d = \mathbf{n}\,(D_d - D_g)\,, \tag{3}$$

and considering material permittivity:

$$\rho_d = \mathbf{n}\varepsilon_0\,(\varepsilon_r E_d - E_g)\,. \tag{4}$$

The dynamics of surface charge ρ_d is governed by a superposition of current components attributed to the dielectric bulk side J_b, void gas side J_g and surface part denoted as J_d [31]:

$$-\frac{\partial \rho_d}{\partial t} = \mathbf{n}J_b + \mathbf{n}J_g + \mathbf{n}J_d\,. \tag{5}$$

The current J_b is determined by bulk void side conductivity γ_b:

$$J_b = \gamma_b E. \tag{6}$$

The current J_g refers to a gaseous side of the interface and combines the electron and ion mobility μ and diffusivity D $F(\mu, D)$:

$$\mu J_g = F(D)\cdot E. \tag{7}$$

The surface current J_d is related to a usually non-linear material surface conductivity γ_d and the tangential component of electric field E_x:

$$J_d = \gamma_d\,(E_x)\cdot E_x\,. \tag{8}$$

The interplay of those current components results in surface charge accumulation and decay.

3. METHODOLOGY AND ANALYTICS OF CHOPPED SEQUENCE

Partial discharges may appear in all dielectric insulation systems, i.e. in solid, liquid and gaseous environments. In PD-based diagnostics of high-voltage electrical insulation, the phase-resolved PD analysis (PRPDA) is an established tool [2, 23]. The PRPDA methodology is graphically highlighted in Fig. 2. This technique allows for the acquisition of individual PD pulses with reference to the phase angle of the applied high voltage. It relies on coupled two-dimensional multichannel analyzers, one responsible for magnitude quantization and the second for scaling the time axis into a phase position. Since PD physical processes indicate a statistical behavior, a method based on phase-resolved PD acquisition can present various PD patterns corresponding to the different underlying physical phenomena. Thus, the PD pattern contains collections of individual partial discharge events superimposed on one HV

period. The third dimension reflects the statistical PD distribution. Chopped partial discharge (CPD) methodology introduces a new diagnostic approach, providing a real-time insight into PD charge dynamics. The decaying charge resulted in the electric field variation from the deposited and accumulated charges from the previous PD events. Surface conditions impact in this way the so-called memory effects associated with the behavior of subsequent discharges [26].

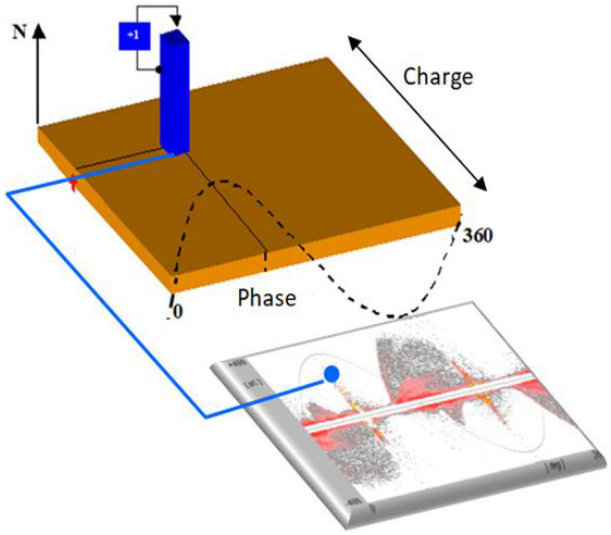

Fig. 2. Methodology of partial discharge phase-resolved acquisition

The presented CPD method allows to assess various mechanisms such as charge neutralization and conduction and is based on the analysis and evolutions of phase-resolved PD images. To explore the individual's charge dynamics, subsequent HV periods are put aside by an introduced artificial gap in the form of a time delay. The partial discharge mechanism in the void strongly depends on the electric field level [3, 4, 7]; thus, the entire dielectric structure's location and high voltage are applied. After the occurrence of an individual discharge event, the electrons from the streamer channel deposited on the void walls undergo decay. Depending on the material properties, they may be trapped or discharged on the void surface. The visualization of the CPD sequence along with underlying charge decay processes is shown in Fig. 3. The graphic is given purely for illustrative purposes and is not to scale, neither in magnitude nor time. As indicated in Fig. 3, the duration of a single epoch t_e, having both packet and delay time as a multiple of period T, is given by:

$$t_e = n \cdot T + k \cdot T = T(n+k), \tag{9}$$

where n is the multiple of base period and k is the delay multiple. Hence the fill factor ff, used further in the chopped sequence definition, has a form:

$$ff = \frac{n \cdot T}{t_e} = \frac{n}{n+k}. \tag{10}$$

The epoch is repeated accordingly to the duration of the whole measurement time to obtain the statistical representation in the

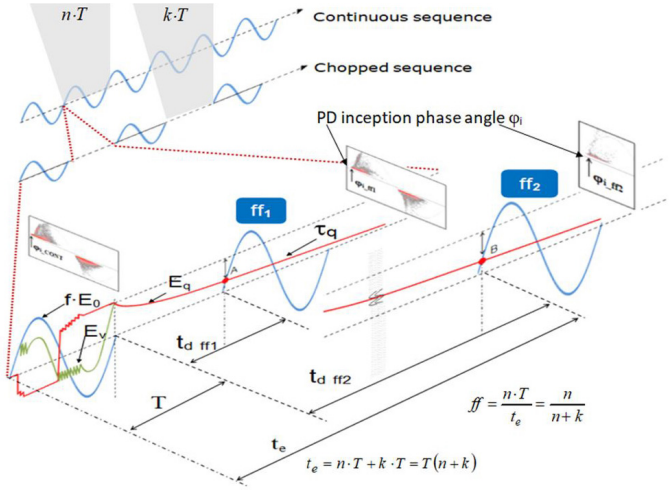

Fig. 3. Visualization of chopped partial discharge (CPD) sequence of two runs with different time delays $t_{d\_ff_1}$ and $t_{d\_ff_2}$ along with underlying charge decay processes; T – period of base waveform; ff_1, ff_2 – fill factors; t_d – delay time, t_e – duration of the epoch; fE_0 – background electric field in the void; E_v – electric field inside void, E_q – electric field due to deposited charges by PD, τ_q – decay time, k – delay multiple, n – multiple of base periods

form of phase-resolved PD pattern. At strongly chopped sequence, i.e. long duration of the delay time, the measurement time should be usually prolonged to obtain a representative number of active base periods.

For the sake of transparency and clarity, partial discharges are denoted only in the first HV period in Fig. 3. The two separate traces corresponding to fill factors ff_1 and ff_2 with time delays (denoted as $t_{d\_ff_1}$ and $t_{d\_ff_2}$, respectively) are superimposed in the plot.

The charge build-up inside the void results from PD streamers and is represented by electric field E_q. The important moment occurs after the last discharge during the period at a negative half-period (in case of a sequence start with positive polarity), when electric field E_q starts to decay. The introduced chopped period within the sequence with delay time allows the progress of this decay to be externally monitored. At the beginning of the consecutive period, the decay of field E_q results in the deficiency of an internal field for PD inception.

The decayed "portion" of E_q field is compensated by the external field jump exposed by the partial discharge inception phase shift (ϕ_{iCONT} towards ϕ_{iff_1} and ϕ_{iff_2}) as depicted in phase-resolved PD patterns. The inception phase angle of the chopped PD patterns, treated as a quantitative indicator, is determined directly from the PRPD images. The proper and exact determination of decay time requires precise measurement of the phase angle positions. In case of high values of fill factors, the measurement time should be extended accordingly to safeguard a representative number of active periods.

The electric field inside void E_v is a superposition of applied external field E_0, corresponding to the external high voltage, which is transposed according to the field distribution and the shape of the void by the factor f and internal field E_q created by

the accumulated charges deposited on the void surface during the previous events:

$$E_v = f \cdot E_0 + E_q(\tau_q), \tag{11}$$

where τ_q represents the decay time constant of the E_q field in the void.

Surface charge field E_q is directly proportional to the accumulated and deployed charges by the discharge events on a void surface $E_q \sim q$ and can be expressed as a decaying function of time:

$$E_q(t) = E_{q_0} \cdot \exp\left(\frac{-t}{\tau_q}\right), \tag{12}$$

where E_{q_0} is the initial charge value, while τ_q represents the cumulative charge q decay due to surface recombination and trapping as well as bulk conduction, neutralization, and other drifts.

$DEvff_1$ and $DEvff_2$ denote the E_v field drop in the void (Fig. 3), respectively at points A and B. Comparing the time decay of electric field E_q for continuous (E_{q_CONT}) and the chopped sequence with fill factor ff_n at the same external high voltage, one obtains the following equations:

$$E_{v\_\mathrm{CONT}} = E_{q\_\mathrm{CONT}} + f \cdot E_0, \tag{13}$$

$$E_{v\_ff_n} = E_{q\_ff_n} + f \cdot E_0. \tag{14}$$

The difference of the electric fields will be equal to:

$$\Delta E_v = E_{v\_\mathrm{CONT}} - E_{v\_ff_n} \tag{15}$$

Comparing this value for the time moment t_{ffn} resulting from the chopped sequence with the n-th fill factor, one obtains:

$$\Delta E_v = E_{q_0} - E_{q_0} \cdot e^{-t_{ffn}/\tau_q} = E_{q_0} \cdot \left(1 - e^{-t_{ffn}/\tau_q}\right). \tag{16}$$

The above decay of field E_q is compensated by the voltage surplus manifested by a PD inception phase shift of high voltage $\Delta\phi i$ relative to the inception phase angle $\varphi_{i\_\mathrm{CONT}}$ in the sinusoidal sequence:

$$\Delta\varphi_i = \varphi_{i\_ffn} - \varphi_{i\_\mathrm{CONT}}. \tag{17}$$

The partial discharge inception voltage surplus is obtained from the corresponding inception phase angles for the chopped and continuous sequences:

$$\Delta U_i = U_0 \cdot \left(\sin\left(\varphi_{i_{ffn}}\right) - \sin(\varphi_{i\_\mathrm{CONT}})\right). \tag{18}$$

Assuming a proportionality factor k between the internal field in the void E_v and the external field fE_0 caused by the external voltage, one obtains:

$$\Delta E_v = k \cdot \Delta U_i. \tag{19}$$

Thus, in general form,

$$E_{q_0}\left(1 - e^{-t_{ffn}/\tau_q}\right) = kU_0\left(\sin\left(\varphi_{i_{ffn}}\right) - \sin(\varphi_{i\_\mathrm{CONT}})\right). \tag{20}$$

The above equation has two unknown elements (E_{q_0} and τ_q). To find time constant τ_q, two measurements should be performed corresponding to two time moments (i.e. fill factors ff_1 and ff_2) as stated denoted below:

$$E_{q_0}\left(1 - e^{-t_{ff_1}/\tau_q}\right) = kU_0\left(\sin\left(\varphi_{i_{ff_1}}\right) - \sin(\varphi_{i\_\mathrm{CONT}})\right), \tag{21}$$

$$E_{q_0}\left(1 - e^{-t_{ff_2}/\tau_q}\right) = kU_0\left(\sin\left(\varphi_{i_{ff_2}}\right) - \sin(\varphi_{i\_\mathrm{CONT}})\right). \tag{22}$$

The system of equations (21) and (22), can be solved using two approaches. One based on analytic transformations will yield following solution [28]:

$$\tau_q = -\frac{t_{ff_1}}{\ln\left(1 - \dfrac{2 \cdot a \cdot \left(t_{ff_2} \cdot a - t_{ff_1} \cdot b\right)}{\left(t_{ff_1} \cdot b^2 - t_{ff_2} \cdot a^2\right)}\right)}. \tag{23}$$

The second solution is based on the application of a numerical solver, applied to an equation (24), obtained after dividing both sides of equations (21) and (22):

$$\frac{\left(1 - e^{-t_{ff_1}/\tau_q}\right)}{\left(1 - e^{-t_{ff_2}/\tau_q}\right)} = \frac{\sin\left(\varphi_{i_{ff_1}}\right) - \sin(\varphi_{i\_\mathrm{CONT}})}{\sin\left(\varphi_{i_{ff_2}}\right) - \sin(\varphi_{i\_\mathrm{CONT}})}. \tag{24}$$

In the above equation, τ_q is an entangled unknown and can only be determined numerically, assuming that the following parameters t_{ff_1}, t_{ff_2}, $\varphi_{i_{ff_1}}$, $\varphi_{i_{ff_2}}$, $\varphi_{i\_\mathrm{CONT}}$ are measured. The calculations of the time constant presented in this paper are based on the numerical solution of equation (24). The solver performs the calculations until a certain predefined error level is obtained.

4. INSTRUMENTATION AND MEASUREMENT SETUP

The chopped sequence and partial discharge measurements were performed in a setup presented in Fig. 4. The waveform generator delivered a programmed CPD sequence and controlled the high voltage amplifier (TREK 20/20B). The protection and filtering impedance $Z = 480$ kΩ was placed in a HV supply path. A coupling capacitor $C_k = 1100$ pF was connected parallel to the specimen denoted as C_x. The measurements were executed at frequency 50 Hz of high voltage. The base period was equal to $T = 20$ ms, and the total number of periods within exemplary measuring time $t_m = 60$ seconds was 3000. According to the selected fill factor, the number of active periods in the chopped PD sequence will be reduced. The chopped sequence consists of a base period T followed by delay time t_d. The partial discharge detection was carried out in a wideband mode according to IEC 60270 standard. The detected PD signal from coupling impedance Z_m was inserted into the signal conditioning unit (SCU) containing filters and a preamplifier. The ICMsystem (Power Diagnostix) connected to a host computer via a GPIB bus was used for a phase-resolved PD acquisition. The recording of PD pulses was synchronized with zero crossings of testing voltage and accumulated in 256×256 matrix (2 bytes depth). The synchronization signal for PD acquisition

(including phase compensation caused by elements of HV circuit) was obtained from a programmable generator. The high voltage signal was monitored using a resistive divider depicted as R_1 and R_2.

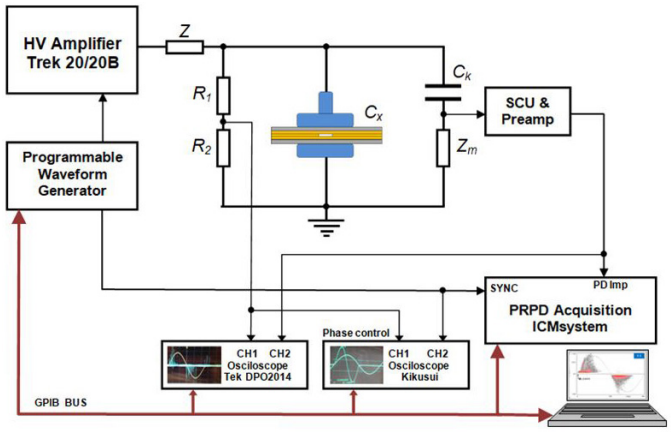

Fig. 4. Measuring setup for chopped PD acquisition: R_1, R_2 – resistive divider (1000:1); C_x – specimen; C_k – coupling capacitor (1.100 pF); Z_m – measuring impedance; SCU – signal conditioning unit and preamplifier; Z – protection and filtering impedance (480 kΩ)

The experiments were carried out on model specimens containing embedded void filled with air at atmospheric pressure. The geometry of the specimen is shown in Fig. 5. A layer of insulating material formed the void with a circular void (radius 5 mm, thickness 0.24 mm) clamped between two glass plates (each 2 mm thick). The electrode arrangements consisted of plain stainless steel electrodes. The electrodes were 40 mm in diameter, with an end curvature of an 8 mm. Before the experiments, the specimens were cleaned by isopropanol, dried, and discharged in a grounded alufoil arrangement. The measurements were performed at room temperature.

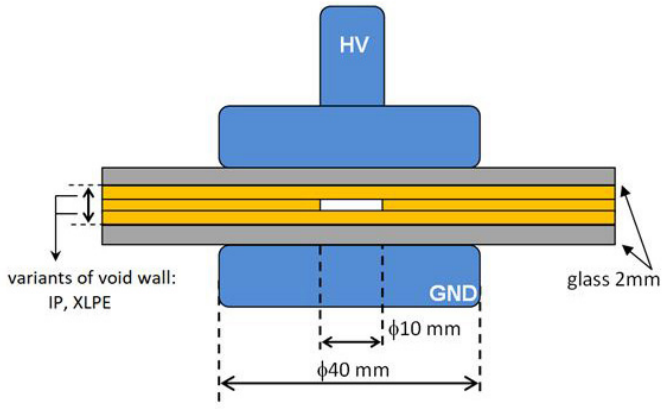

Fig. 5. The geometry of the specimen with embedded void

5. RESULTS AND DISCUSSION

Two materials characterized by different physical properties such as surface resistivity and morphology, i.e., cross-linked polyethylene (XLPE) and insulating paper (IP), were used for the void walls in the presented experiments. The geometrical layer structure of the specimen is presented in Fig. 5. The internal embedded void had a diameter of 10 mm and a thickness of 0.24 mm. XLPE is used for power cable insulation; insulating paper is the traditional approach in high-voltage insulation applied as oil-impregnated insulation for cables or transformers.

The internal inception voltage U_{o_int} inside a void with reference to the external voltage U_0 can be recalculated according to the formula:

$$U_{0\,int} = \frac{U_0}{\dfrac{d_1}{d_3 \cdot \varepsilon_g} + \dfrac{d_2}{d_3 \cdot \varepsilon_{ins}}}, \tag{25}$$

where:

d_1 – thickness of glass plates;
d_2 – thickness of insulating material;
d_3 – thickness of air void;
ε_g – dielectric permittivity of glass;
ε_{ins} – dielectric permittivity of insulating material.

The main dispersion of the inception voltage between specimens was related to the dielectric permittivity and thicknesses of the wall materials. The measured dielectric permittivity values of the insulating materials were equal to: $\varepsilon_{\mathrm{XLPE}} = 2.2$ and $\varepsilon_{\mathrm{IP}} = 3.2$. For measured inception voltage $U_0 = 5$ kV, the internal PD inception voltage recalculated according to equation (23) is 1.1 kV. This value corresponds well to the level of Paschen breakdown voltage, which yields around 0.8 kV in this case of pressure and distance. The presented measurements were obtained at a voltage of $1.2\,U_0$.

The calculations of the post-charge decay in the void was carried according to the methodology presented above. The CPD sequence was programmed with a time delay t_d within a range of 20–2540 ms, which corresponds to fill factors *ff* of 1:2 to 1:128.

The variation of the fill factor *ff* in a chopped sequence results in a modulation of the PD positive inception phase angle. The observations have confirmed that the negative inception phase angle was very stable despite t_d variations. The CPD measurements were carried out at a high voltage equal to 6 kV $(1.2 \cdot U_0)$, where U_0 corresponds to the PD inception voltage at a continuous sequence. The PD patterns for the two void wall materials (cross-linked polyethylene and insulating paper) are presented in Fig. 6 and Fig. 7.

The PD inception phase angle ϕ_i for the continuous sequence and chopped mode with fill factors of 1:2 to 1:128 is shown in Table 1. The positive PD inception phase angle is marked as $\phi_{i\,\mathrm{cont}}$ for the continuous case and as $\phi_{i\mathrm{CPD}}$ in the chopped mode.

Table 1

Inception phase angle ϕ_i [°] for different void wallmaterials as well as continuous and chopped modes with fill factors 1:2 to 1:128

ff	CONT	1:2	1:16	1:64	1:128
t_d [ms]	0	20	300	1260	2540
IP [°]	6	14	16	–	–
XLPE [°]	0	1	–	–	21

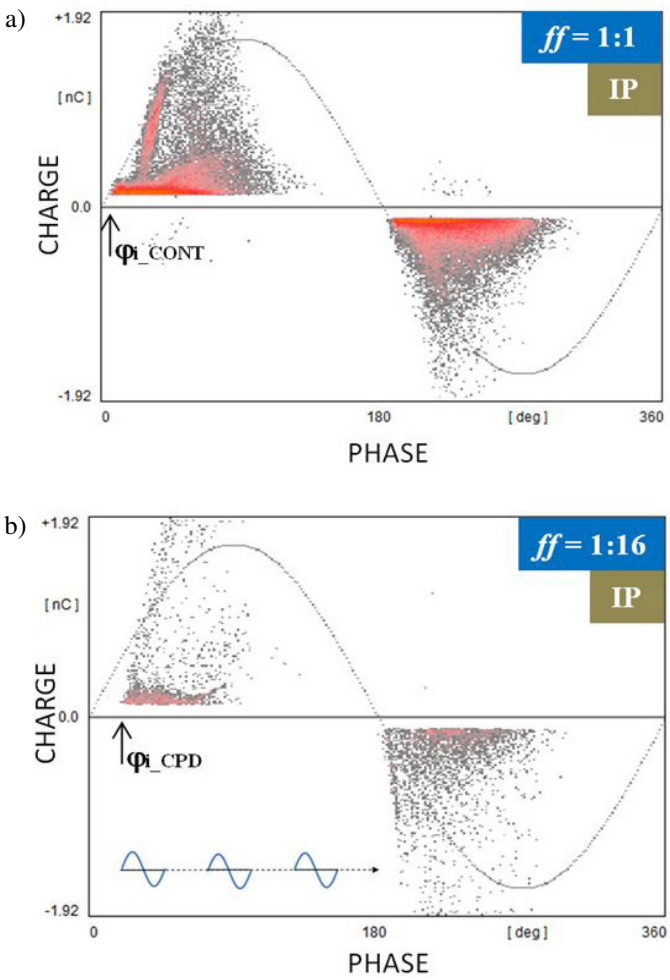

Fig. 6. PD pattern obtained in void with insulating paper wall at: a) sinusoidal voltage in continuous mode; b) $ff = 1{:}16$ ($t_d = 300$ ms)

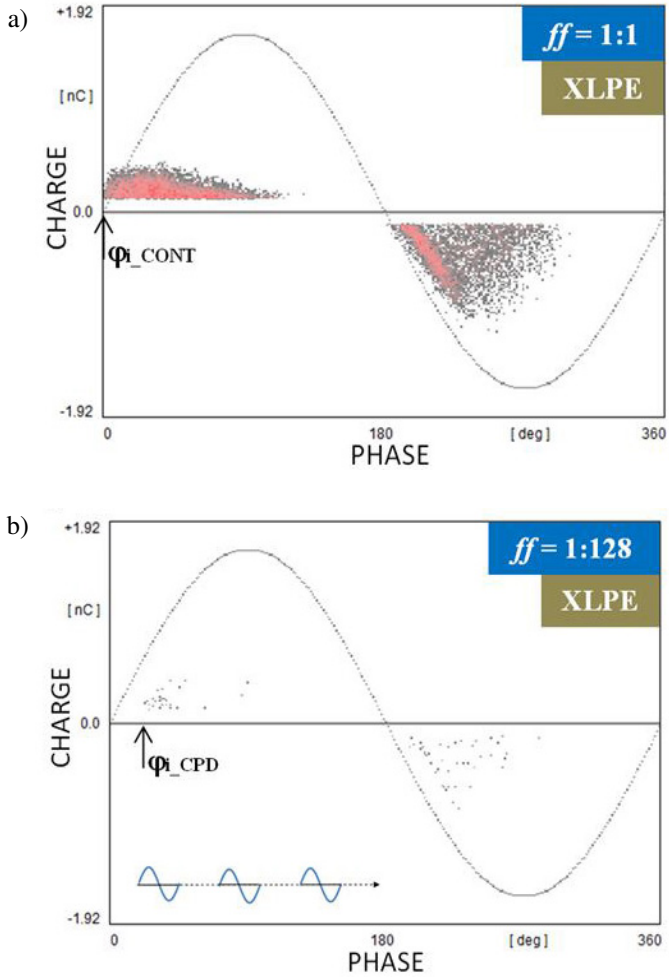

Fig. 7. PD pattern obtained in void with XLPE wall at: a) sinusoidal voltage in continuous mode; b) $ff = 1{:}128$ ($t_d = 2.540$ ms)

The PD patterns for the insulating paper specimen are shown in Fig. 6. The partial discharge image acquired at a continuous sinusoidal voltage (in this case, time delay in CPD sequence $t_d = 0$) is shown in Fig. 6a and fill factor 1:16 in Figs. 6b, respectively. In this case, the inception phase shift yields 10° when comparing the difference between a continuous sequence and one delayed by 300 ms. The PD patterns for the XLPE specimen are shown in Fig. 7. The PD pattern obtained at continuous sinusoidal voltage is shown in Fig. 7a and for fill factors 1:128 in Figs. 7b, respectively. The inception phase shift difference for the XLPE void walls is equal to 21° between the continuous sequence and the sequence delayed by 2540 ms.

According to CPD methodology, the comparison of PD inception phase angles between the continuous and chopped sequences is used as an indicator for calculating the internal charge time decay in the void. The electric field drop of the internal void is compensated by the delayed inception phase angle, resulting in a higher external field.

The mechanism of inception phase shift is described in [18, 28]. A comparison of time decay τ_q of the E_q field obtained for the investigated void wall materials is presented in Table 2. The charge decay time is calculated applying the methodology presented in the previous section. The calculation was based on the measured PD inception angles and the time parameters of the CPD sequence.

Table 2
Comparison of time constant τq obtained for various void wall materials

Specimen	Charge decay time τ_q [ms]
Insulating paper	12
XLPE	407

The charge neutralization and conduction mechanisms post discharge period on the void surface contribute to the E_q electric field decay with a resultant time constant τ_q. In both cases, the neutralization conditions in gaseous space are similar. The main difference is related to the surface and bulk conductivity. As calculated using CPD method, the insulating paper void yields a charge time decay of around 12 ms, whereas for XLPE the charge time decay is 407 ms. The electrical properties of the IP and XLPE specimens, specifically the surface and volume resistivity and relative dielectric permittivity, are shown in

Table 3. Both surface and volume resistivity differ in one order of magnitude in the case of both materials.

Table 3
Properties of IP and XLPE specimens

	IP	XLPE
Surface resistivity [Ω]	$2.0 \cdot 10^{12}$	$2 \cdot 10^{13}$
Volume resistivity [Ω· m]	$4.6 \cdot 10^{13}$	$6 \cdot 10^{14}$
Relative dielectric permittivity	3.2	2.2

The void wall surface resistivity influences the transport of charges; i.e., low resistivity tends to reduce the E_q field, while higher resistivity fosters the preservation of the charge reservoir and simultaneously contributes to the time lag and initial inception conditions. The shorter surface charge decay through conduction causes the electron generation rate to decrease much faster, increasing the statistical time lag. The inception effects are visible in the chopped PD pattern. In such a case, they are shifted forward in phase comparing with the corresponding sinusoidal pattern. The distinct effect of investigated materials' surface conductivity (order of magnitude difference) is revealed in measured using CPD method charge decay times.

6. CONCLUSIONS

Diagnostic methodologies are of fundamental importance for operational strategies of electrical devices, both in the power grid and in industrial applications. This paper reports about a novel approach based on partial discharge analysis applied to high voltage electrical insulation. Especially dynamics of charges deposited by partial discharges is explored applying a chopped sequence. The applications refer to microvoids occurring in solid insulating systems or at the interfaces. The experiments were carried out on an embedded void having two different wall dielectric materials. The underlying physical phenomena of post discharge charge transport are analyzed. The assessment is performed using phase-resolved PD patterns acquired in a designed chopped sequence. The CPD method provides quantitative insight into post discharge charge decay processes due to fluctuations of deposited and accumulated charges. The assessment indicator is based on the comparison of partial discharge inception angle between chopped sequence and continuous run. In the case of CPD the sequences for different fill factors are executed. The experiments have shown that materials with distinctive surface conductivity revealed adequately different charge decay time dynamics. The detailed analysis yields time constant of walls charge decay for insulating paper equal to 12 ms and for cross-linked polyethylene 407 ms. The CPD method may be further used to investigate streamer physics inside bounded cavities in the form of voids. The long-term PD reaction on insulating material results in surface deterioration and might be monitored using a chopped methodology. The presented method is still in the early research stadium but offers high potential in diagnostics applications.

REFERENCES

[1] T. Tanaka and Y. Ikeda, "Internal discharges in polyethylene with an artificial cavity," *IEEE Trans. Power Apparatus Syst.*, vol. 90, no. 6, pp. 2692–2702, 1971.

[2] B. Fruth and L. Niemeyer, "The importance of statistical characteristics of partial discharge data," *IEEE Trans. Electr. Insul.*, vol. 27, no. 1, pp. 60–69, 1992.

[3] L. Niemeyer, "Generalized approach to partial discharge modelling," *IEEE Trans. Dielectr. Electr. Insul.*, vol. 2, no. 4, pp. 510–528, 1995.

[4] H. Illias, G. Chen, and P.L. Lewin, "Partial discharge behavior within a spherical cavity in a solid dielectric material as a function of frequency and amplitude of the applied voltage," *IEEE Trans. Dielectr. Electr. Insul.*. vol. 18, pp. 432–443, 2011, doi: 10.1109/TDEI.2011.5739447.

[5] M.A. Saleh, S.S. Refaat, M. Olesz, H. Abu-rub, and J. Guźiński, "The effect of protrusions on the initiation of partial discharges in XLPE high voltage cables," *Bull. Pol. Acad. Sci. Tech. Sci.*, vol. 69, no. 1, 2021, doi: 10.24425/bpasts.2021.136037.

[6] M. Florkowski, M. Kuniewski, and P. Zydroń, "Partial discharges in HVDC insulation with superimposed AC harmonics," *IEEE Trans. Dielectr. Electr. Insul.*, vol. 27, no. 6, pp. 1875–1882, 2020.

[7] G.C. Crichton, P.W. Karlsson, and A. Pedersen, "partial discharges in ellipsoidal and speroidal voids," *IEEE Trans. Electr. Insul.*, vol. 24, no. 2, pp. 335–342, 1989.

[8] I.W. McAllister, "Decay of charge deposited on the wall of gaseous void," *IEEE Trans. Electr. Insul.*, vol. 27, no. 6, pp. 1202–1207, 1992.

[9] T. Tanaka and M. Uchiumi, "Two kinds of decay time constants for interfacial space charge in polyethylene-laminated dielectrics," in *Proc. Conf. on Electr. Insul. Dielectri. Phenom. (CEIDP)*, 1999, pp. 472–475.

[10] T. Mizutani, Y. Taniguchi, and M. Ishioka, "Charge decay and space charge in corona-charged LDPE," in *Proc. 11th International Symposium on Electrets*, 2002, pp. 15–18.

[11] B. Florkowska, "Partial discharge measurements with computer aided system in polyethyleneterephthalate and polypropylene films," in *Proc. High voltage engineering. 8th International Symposium*, Yokohama, Japan, 1993, pp. 41–44.

[12] H.J.M. Blennow, M.L.A. Sjoberg, M.A.S. Leijon, and S.M. Gubanski, "Effects of charge accumulation in a dielecric covered electrode system in air," in *Proc. IEEE Conf. Electr. Insul. Dielectr. Phenom. (CEIDP)*, 1999, pp. 484–487.

[13] K. Wu *et al.*, "Contribution of surface conductivity to the current forms of partial discharges in voids," *IEEE Trans. Dielectr. Electr. Insul.*, vol. 12, no. 6, pp. 1116–1124, 2005.

[14] L.A. Dissado *et al.*, "Decay of space charge in a glassy epoxy resin following voltage removal," *IEEE Trans. Dielectr. Electr. Insul.*, vol. 13, no. 4, pp. 903–916, 2006.

[15] Y. Serdyuk and S. Gubanski, "Computer modeling of interaction of gas discharge plasma with solid dielectric barriers," *IEEE Trans. Dielectr. Electr. Insul.*, vol. 12, pp. 725–735, 2005, doi: 10.1109/tdei.2005.1511098.

[16] S. Kumara, Y.V. Serdyuk, and S.M. Gubanski, "Surface charge decay on polymeric materials under different neutralization modes in air," *IEEE Trans. Dielectr. Electr. Insul.*, vol. 18, no. 5, pp. 1779–1788, 2011.

[17] K. Wu, C. Pan, Y. Meng, Y. Cheng, and M. Ding, "Dynamic behavior of surface charge distribution during partial discharge sequence," *IEEE Trans. Dielectr. Electr. Insul.*, vol. 20, no. 2, pp. 612–619, 2013.

[18] M. Florkowski, B. Florkowska, P. Zydron, "Chopped Partial Discharge Sequence," *IEEE Trans. Dielectr. Electr. Insul.*, vol. 22, no. 6, pp. 3451–3458, 2015.

[19] H.A. Illias, M.A. Tunio, A.H.A. Bakar, H. Mokhlis, and G. Chen, "Partial discharge phenomena within an artificial void in cable insulation geometry: experimental validation and simulation," *IEEE Trans. Dielectr. Electr. Insul.*, vol. 23, no. 1, pp. 451–459, 2016.

[20] J. Kindersberger and C. Lederle, "Surface charge decay on insulators in air and sulfurhexafluorid – Part I: simulation," *IEEE Trans. Dielectr. Electr. Insul.*, vol. 15, no. 4, pp. 941–948, 2008.

[21] M. Florkowski, "Influence of insulating material properties on partial discharges at dc voltage," *Energies*, vol. 13, p. 4305, 2020.

[22] L. Xing, L. Weidong, X. Yuan, C. Weijiang, and B. Jiangang, "Surface charge accumulation and pre-flashover characteristics induced by metal particles on the insulator surfaces of 1100 kV GILs under AC voltage," *High Voltage*, vol. 5, no. 2, pp. 134–142, 2020.

[23] M. Florkowski, *Partial discharges in high-voltage insulating systems – mechanisms, processing, and analytics*, AGH Press, Kraków, 2020.

[24] Y. Luo *et al*., "Dynamics of surface charge and electric field distributions on basin-type insulator in GIS/GIL due to voltage polarity reversal," *High Voltage*, vol. 5, no. 2, pp. 151–159, 2020.

[25] Q. Li *et al*., "Surface charge pattern analysis based on the field-dependent charging theory: a review," *IEEE Trans. Dielectr. Electr. Insul.*, vol. 27, no. 1, pp. 257–269, 2020.

[26] C. Pan *et al*., "Understanding partial discharge behavior from the memory effect induced by residual charges: A review," *IEEE Trans. Dielectr. Electr. Insul.*, vol. 27, no. 6, pp. 1936–1950, 2020, doi: 10.1109/TDEI.2020.008960.

[27] C. Pan *et al*., "The effect of surface charge decay on the variation of partial discharge location," *IEEE Trans. Dielectr. Electr. Insul.*, vol. 23, no. 4, pp. 2241–2249, 2016.

[28] M. Florkowski, B. Florkowska, and R. Włodek, "Investigations on Post Partial Discharge Charge Decay in Void Using Chopped Sequence," *IEEE Trans. Dielectr. Electr. Insul.*, vol. 26, no. 6, pp. 3831–3838, 2017.

[29] M. Florkowski, B. Florkowska, M. Kuniewski, and P. Zydroń, "Mapping of discharge channels in void creating effective partial discharge area," *IEEE Trans. Dielectr. Electr. Insul.*, vol. 25, no. 6, pp. 2220–2228, 2018.

[30] G. Callender, K.F. Goddard, and P.L. Lewin, "Simulating surface charge dynamics," *IEEE Trans. Dielectr. Electr. Insul.*, vol. 28, no. 1, pp. 19–27, 2021.

[31] H. He *et al*., "Simulation of positive streamer propagation in an air gap with a GFRP composite barrier," *High Voltage*, pp. 1–13, 2021, doi: 10.1049/hve2.12112.